†Electronic Supplementary Information

For

Multiresponsive tetrarylethylene-based fluorescent dye with multicolored changes: AIEE properties, acidichromism, Al^{3+} recognition, and applications

Yanqun Mu [a1], Huanhuan Fan [a1], Mengyuan Li [a], Renjie Wang [a]*, Zhao Chen [a], Congbin Fan [a], Gang Liu [a], Shouzhi Pu [a,b]*

[a]*Jiangxi Key Laboratory of Organic Chemistry, Jiangxi Science and Technology Normal University, Nanchang 330013, P. R. China*

[b]*Department of Ecology and environment, Yuzhang Normal University, Nanchang 330103, P. R. China*

*Corresponding author 1: E-mail address: bio-wrj@163.com

*Corresponding author 2: E-mail address:pushouzhi@tsinghua.org.cn

1. Experimental section

1.1 General methods

Unless otherwise stated, all of the chemicals for the synthesis of the **BTAE-PA** were purchased from various commercial sources and without further purification. All solvents were of spectro-grade and purified by distillation prior to use. ^{1}HNMR and ^{13}CNMR spectra were measured on a Bruker AV500M (500 MHz) spectrometer with $CDCl_3$ as the solvent and TMS as an internal standard. Mass spectra were performed using a Agilent 1100 ion trap MSD spectrometer. UV/Vis spectra were tested on Agilent 8454 UV/vis spectrophotometer. Fluorescence spectra were captured by a Hitachi F−4600 spectrophotometer. Quantum yield was measured with Hamamatsu Absolute PL Quantum Yield Spectrometer C11347-11. Melting point was obtained on a WRS-1B melting point apparatus. Luminescent decay experiments were determined by Edinburgh FLS 980 spectrophotometer. The aggregate behaviors of compounds were investigated by scanning electron microscopy (SEM, Zeiss, Sigma). Dynamic light scattering (DLS) studies were performed by Brookhaven NanoBrook 90 Plus. Fluorescent images were obtained on an Olympus FV1000 confocal laser scanning microscope.

1.2 Synthesis

The synthetic route for **BTAE-PA** was shown in Scheme S1. Firstly, 5-(1, 2, 2-triphenylvinyl)thiophene-2-carbaldehyde was synthesized according to the reported methods [S1]. Then, 2-amino-4, 6-dimethylpyrimidine was coupled with 5-(1, 2, 2-triphenylvinyl)thiophene-2-carbaldehyde through the Knovevenagel condensation reaction to give 4, 6-bis-2-(5-(1, 2, 2-triphenylvinyl)thiophene-2-yl)vinyl)pyrimidine-2-amine (**BTAE-PA**). The structure of **BTAE-PA** were confirmed by NMR and HRMS-ESI.

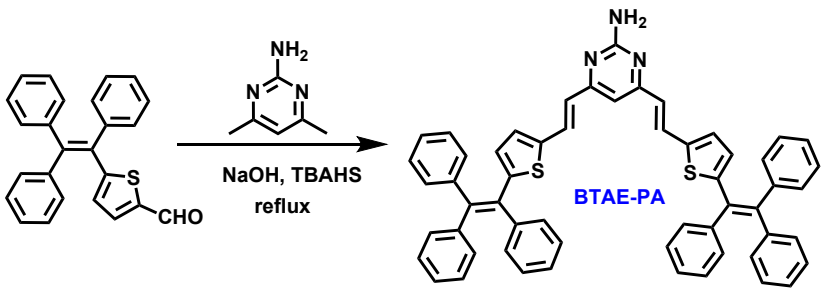

Scheme S1. The synthetic route of **BTAE-PA**.

1.2.1 Synthesis of 4, 6-bis-2-(5-(1, 2, 2-triphenylvinyl)thiophene-2-yl)vinyl)pyrimidine-2-amine (BTAE-PA)

5-(1, 2, 2-Triphenylvinyl)thiophene-2-carbaldehyde (1.00 g, 2.70 mmol) and tetra-*n*-butylammonium hydrogen sulphate (TBAHS, 0.92 g, 2.70 mmol) into a 100 mL three-necked flask, added 60 mL 5 M sodium hydroxide as the solvent. Then, argon was fed into the reaction system and stirred. 2-amino-4, 6-dimethylpyrimidine (0.67 g, 5.40 mmol) was added behind the residual air in the flask was drained, and the reaction continued with oil bath heated to reflux for 5 h at 120 °C. After cooling the mixture solution to the room temperature, the crude product was extracted by dichloromethane, and dried with anhydrous sodium sulfate for 2 h. The crude product was concentrated by rotary evaporation, and purified by column chromatography on silica using petroleum ether / ethyl acetate (*v:v* = 3:1) as the eluent to give 0.80 g **BTAE-PA** as a yellow solid in 36% yield. M. p. 149–150 ℃; Anal. Calcd for $C_{56}H_{41}N_3S_2$ (%): C, 82.02; H, 5.04; N, 5.12; Found: C, 82.05; H, 5.07; N, 5.08; ^{1}H NMR (500 MHz, $CDCl_3$, ppm): δ 4.86 (s, 2H), 6.42 (s, 2H), 6.47–6.45 (t, J = 5.0 Hz, 3H), 6.86 (d, J = 5.0 Hz, 2H), 6.97 (t, J = 5.0 Hz, 4H), 7.06 (d, J = 5.0 Hz, 6H), 7.18 (s, 11H), 7.23 (t, J = 5.0 Hz, 4H), 7.28 (d, J = 5.0 Hz, 4H), 7.65 (s, 1H), 7.68 (s, 1H); ^{13}C NMR (126 MHz, $CDCl_3$, ppm): δ = 108.36, 111.08, 124.62, 126.88, 127.46, 127.80, 127.86, 128.11, 128.71, 129.26, 131.00, 131.03, 131.24, 131.63, 133.99, 141.78, 142.59, 142.93, 143.17, 143.46, 148.77; HRMS-ESI (*m/z*): $[M + H]^+$ Calcd. For ($C_{56}H_{41}N_3S_2^+$), 820.2820, found: 820.2843.

1.3 Figure of Contents

THF-d_8 (top), and HRMS-ESI spectra of **BTAE-PA**+Al^{3+} in acetonitrile (bottom).

Figure S10. (A) Hildebrand-Benesi plot based on the 1:1 ratio between **BTAE-PA** and Al^{3+}, the binding constant for **BTAE-PA** with Al^{3+} was calculated to be 8.30×10^4 L mol^{-1}, and (B) the limit of detection (LOD), LOD is 1.30×10^{-7} mol L^{-1}.

Figure S11. (A) Hildebrand-Benesi plot based on the 1:1 ratio between **BTAE-PA** and Cr^{3+}, the binding constant for **BTAE-PA** with Cr^{3+} was calculated to be 2.90×10^3 L mol^{-1}; (B) the limit of detection (LOD), LOD is 1.50×10^{-7} mol L^{-1}; (C) Changes in ^{1}H NMR spectra of **BTAE-PA** stimuli by different Cr^{3+} concentration in THF-d_8, and (D) HRMS-ESI spectra of **BTAE-PA**+Cr^{3+} in acetonitrile.

Figure S12. (A) Hildebrand-Benesi plot based on the 1:1 ratio between **BTAE-PA** and Fe^{3+}, the binding constant for **BTAE-PA** with Fe^{3+} was calculated to be 5.20×10^3 L mol^{-1}; (B) the limit of detection (LOD), LOD is 8.0×10^{-8} mol L^{-1}; (C) Changes in ^{1}H NMR spectra of **BTAE-PA** stimuli by different Fe^{3+} concentration in THF-d_8, and (D) HRMS-ESI spectra of **BTAE-PA**+Fe^{3+} in acetonitrile.

Figure S13. Absorption and fluorescence spectral changes of **BTAE-PA** by stimulation of Hcy (C = 2.0×10^{-5} mol L^{-1}): (A) absorption changes (inset: the effect of Hcy concentration on absorption intensity at 486 nm); (B) PL intensity changes (inset: the effect of Hcy concentration on emission intensity at 653 nm, λ_{ex} = 400 nm).

Figure S14. Cytotoxicity of **BTAE-PA** on HeLa cells evaluated by the MTT assay for 24 h.

Figure S15. Fluorescent confocal microscopy images of HeLa cells incubated in PBS buffers with various pH (5.0→8.0) and stained with 20 μM of **BTAE-PA**: (A_1–A_4) dark field images, (B_1–B_4) bright field images, (C_1–C_4) overlaid of dark and bright field images, scar bars: 50 μm.

1.4 Table of Contents

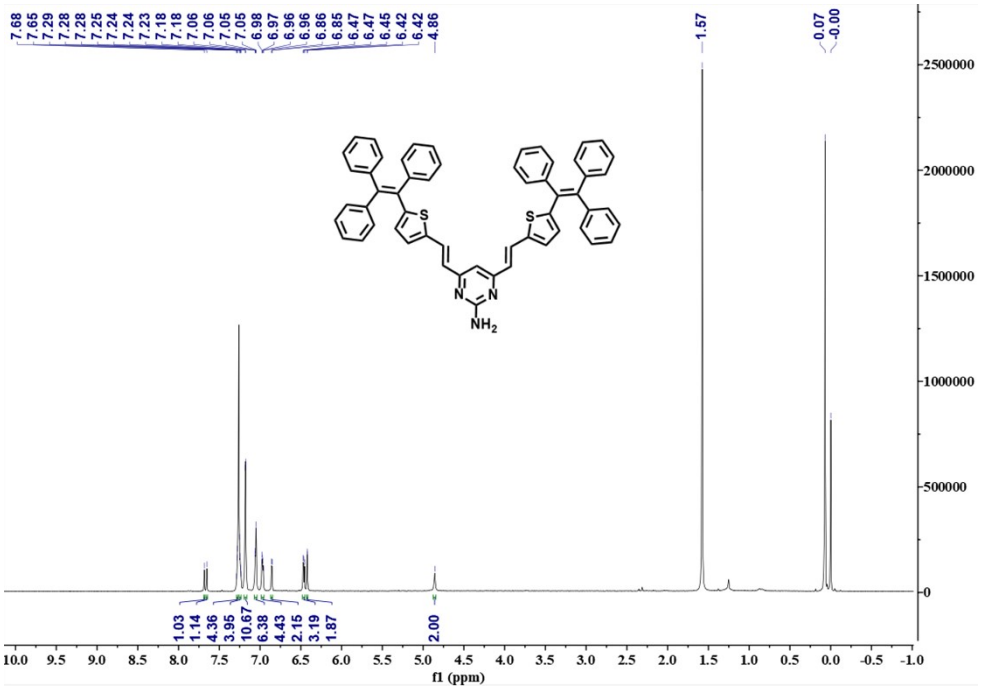

(A)

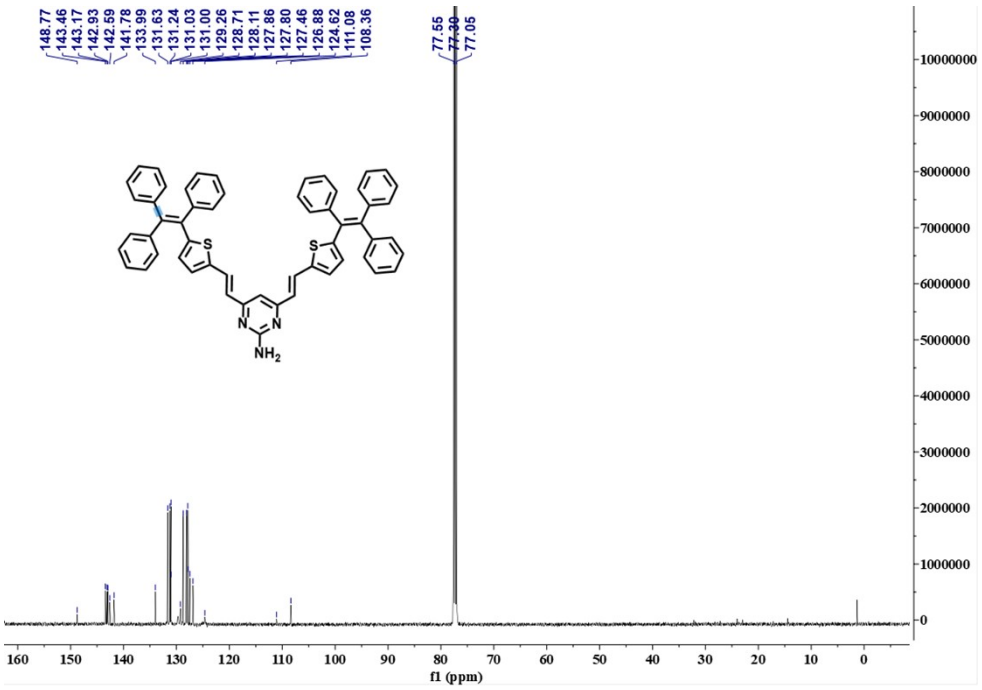

(B)

Figure S1. NMR spectra data for **BTAE-PA** in $CDCl_3$: (A) ^{1}H-NMR spectrum; (B) ^{13}C-NMR spectrum.

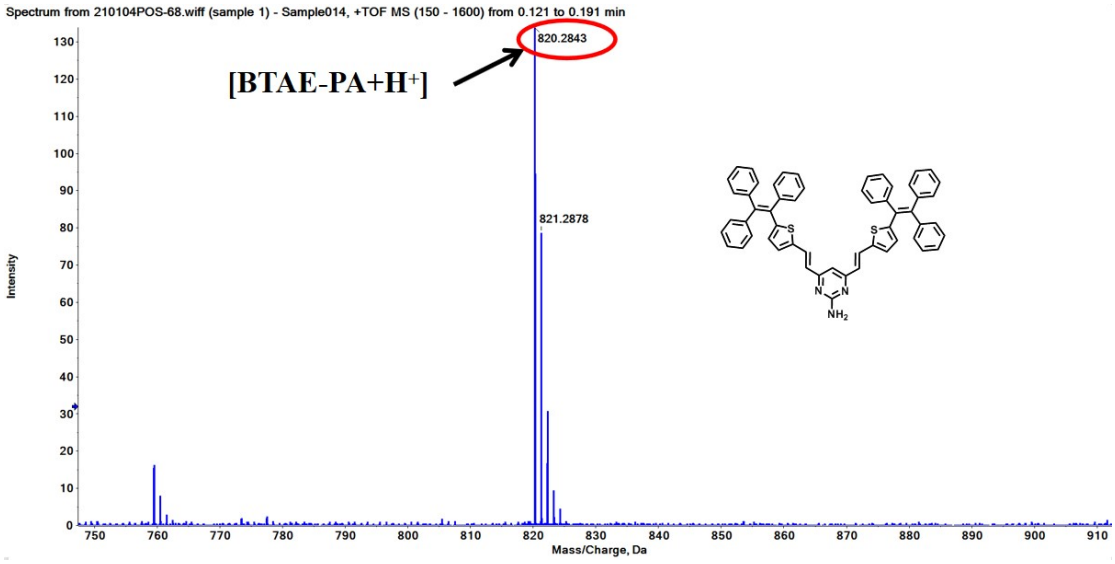

Figure S2. HRMS-ESI spectra of **BTAE-PA** in acetonitrile.

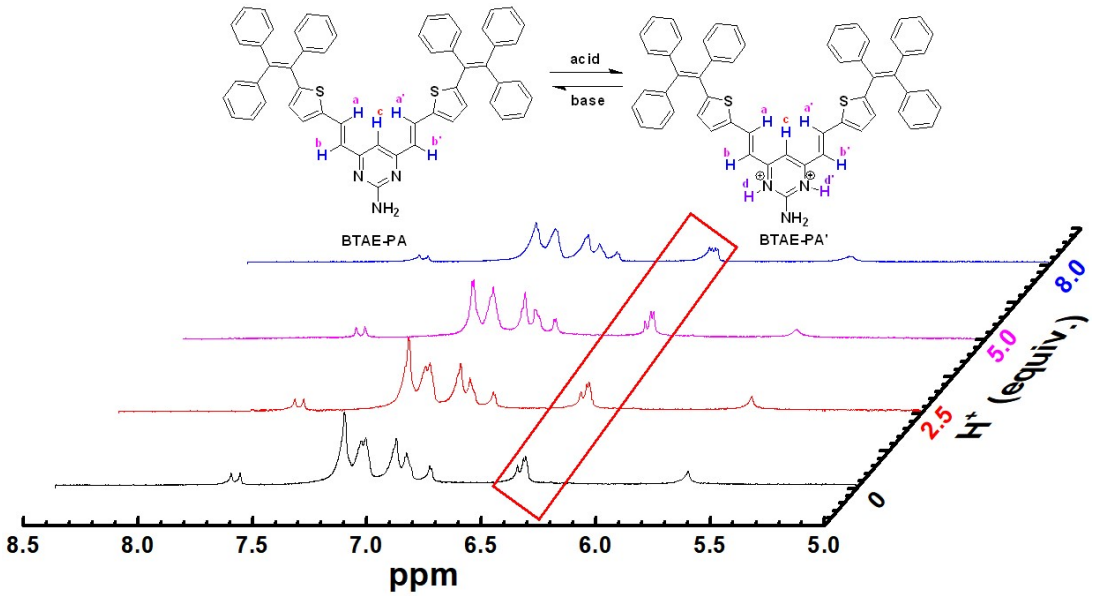

Figure S3. Changes in ^{1}H NMR spectra of **BTAE-PA** stimuli by different H^{+} concentration in THF-d_8.

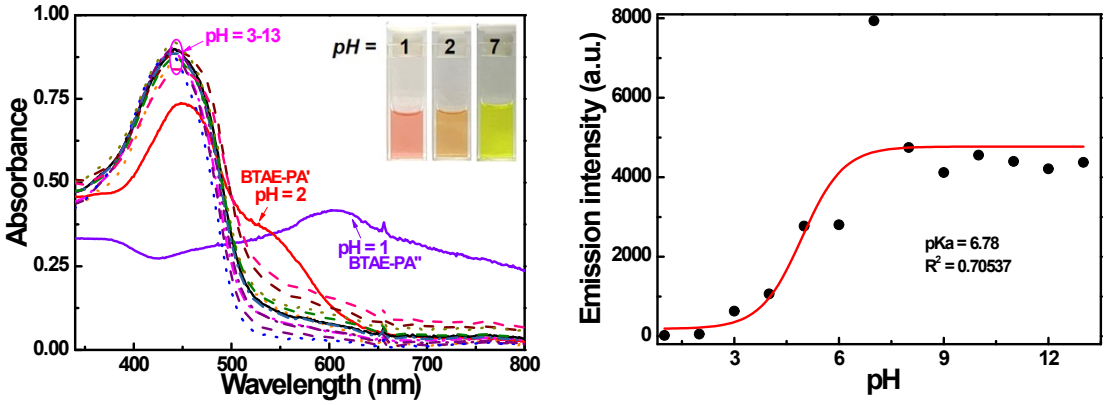

Figure S4. (A) Absorption spectra and color changes of **BTAE-PA** aggreates in different pH value solutions, and (B) change of the fluorescence spectra of **BTAE-PA** with increasing pH from 1.0 to 13.0: sigmoidal fitting of the pH-dependent fluorescence intensity at 591 nm.

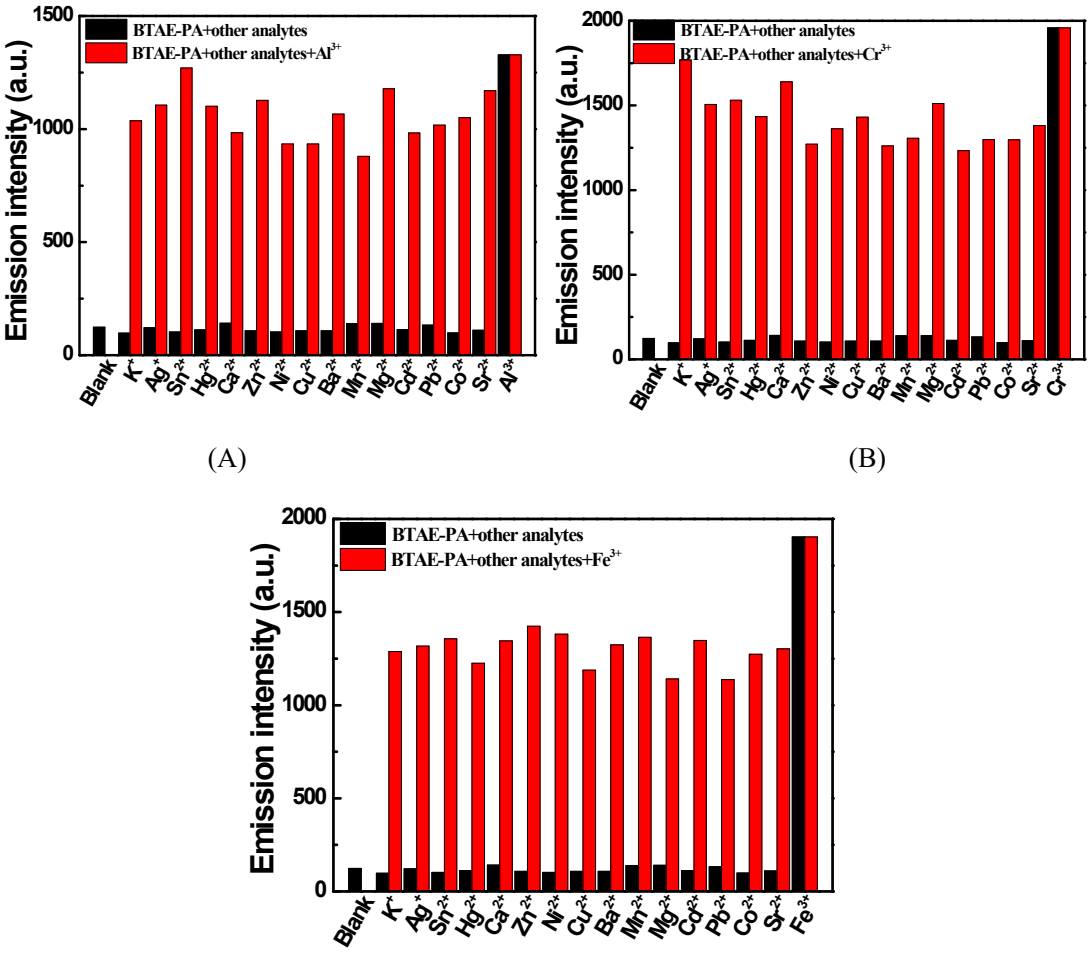

(A) (B)

(C)

Figure S5. Competitive test showing the fluorescence response of **BTAE-PA** to different metal ions (5.0 equiv.) in THF (C =2.0 × 10^{-5} mol L^{-1}). Black bars: **BTAE-PA** with various metal ions; red bars: **BTAE-PA** with different competing metal ions and Al^{3+} (A), Cr^{3+} (B), and Fe^{3+} (C).

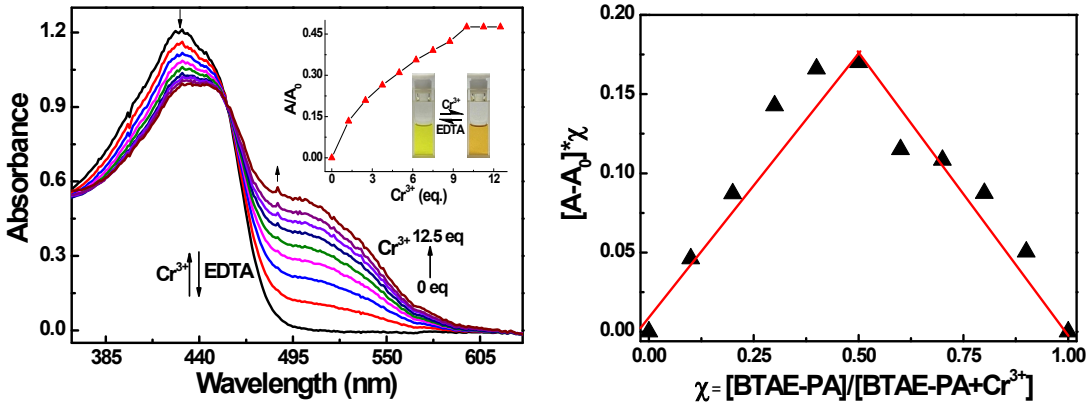

(A) (B)

Figure S6. Absorption spectral changes of **BTAE-PA** by stimulation of Cr^{3+} ($C = 2.0 \times 10^{-5}$ mol L^{-1}): (A) absorption spectral and color changes (inset: the effect of Cr^{3+} concentration on absorption intensity at 486 nm); (B) Job's plot for **BTAE-PA** with Cr^{3+} .

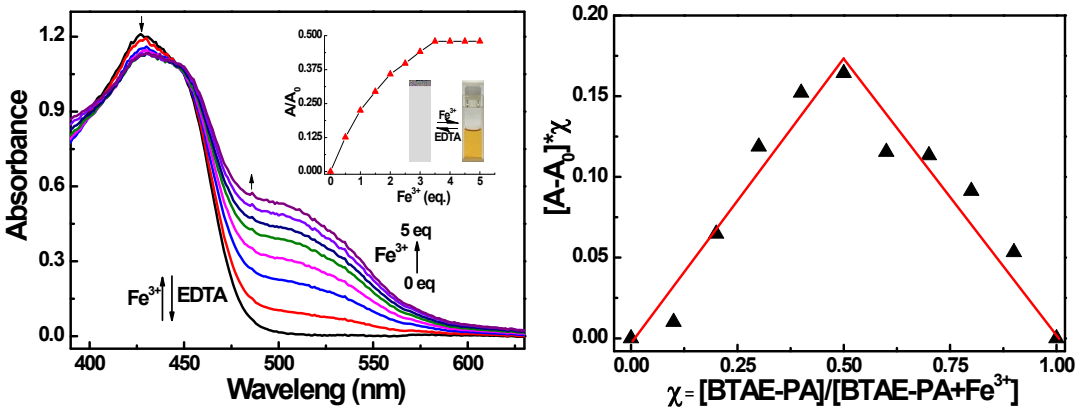

(A) (B)

Figure S7. Absorption spectral changes of **BTAE-PA** by stimulation of Fe^{3+} ($C = 2.0 \times 10^{-5}$ mol L^{-1}): (A) absorption spectral and color changes (inset: the effect of Fe^{3+} concentration on absorption intensity at 486 nm); (B) Job's plot for **BTAE-PA** with Fe^{3+} .

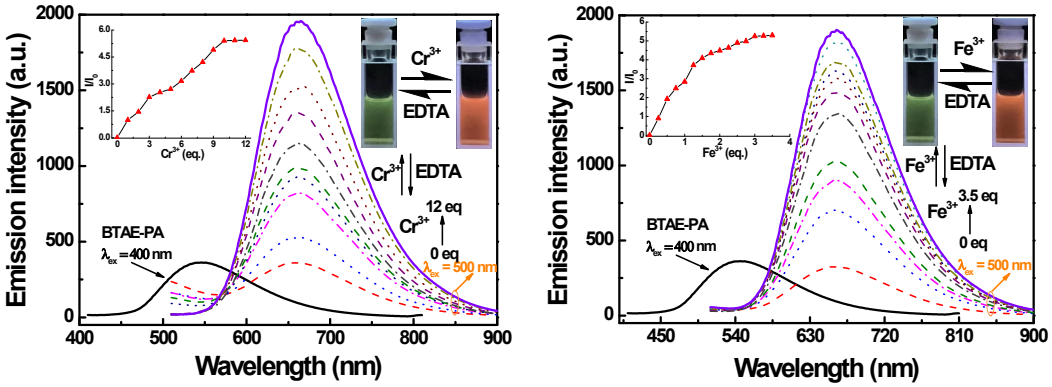

(A) (B)

Figure S8. (A) Emission intensity and color changes (inset: the effect of Cr^{3+} concentration on emission intensity at 665 nm); (B) emission intensity and color changes (inset: the effect of Fe^{3+} concentration on emission intensity at 662 nm).

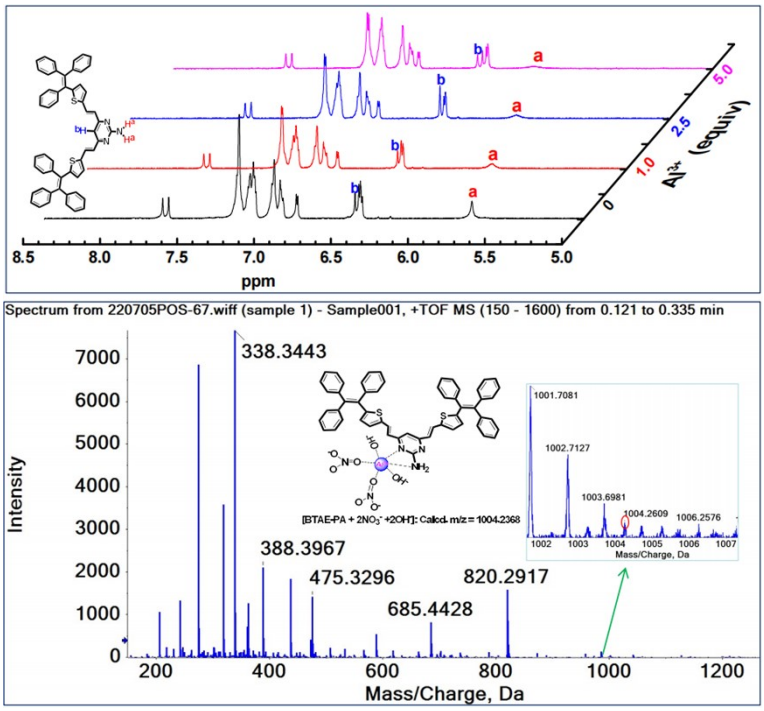

Figure S9. Changes in ^{1}H NMR spectra of **BTAE-PA** stimuli by different Al^{3+} concentration in THF-d_8 (top), and HRMS-ESI spectra of **BTAE-PA**+Al^{3+} in acetonitrile (bottom).

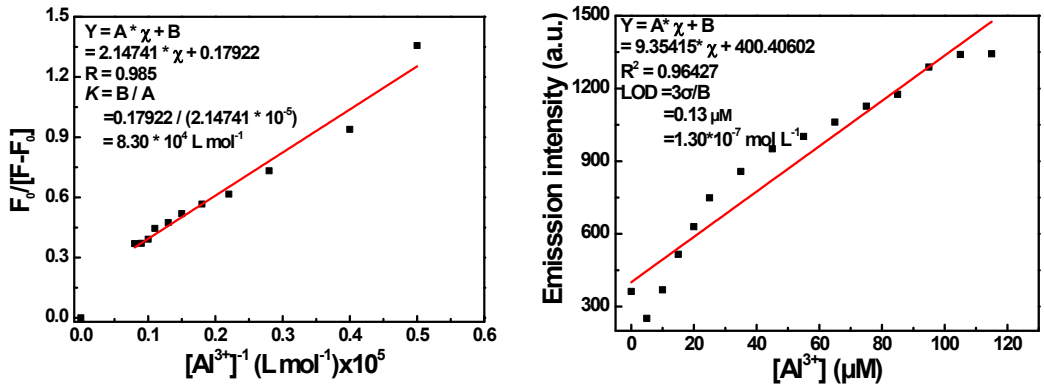

(A) (B)

Figure S10. (A) Hildebrand-Benesi plot based on the 1:1 ratio between **BTAE-PA** and Al^{3+}, the binding constant for **BTAE-PA** with Al^{3+} was calculated to be 8.30×10^4 L mol^{-1}, and (B) the limit of detection (LOD), LOD is 1.30×10^{-7} mol L^{-1}.

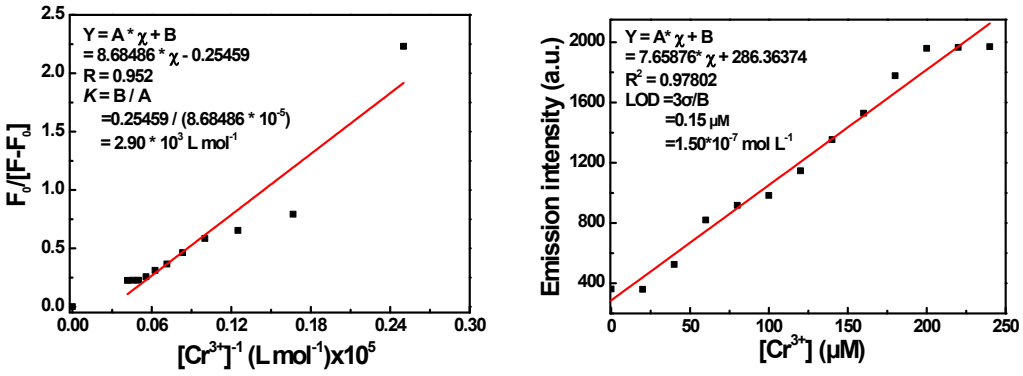

(A) (B)

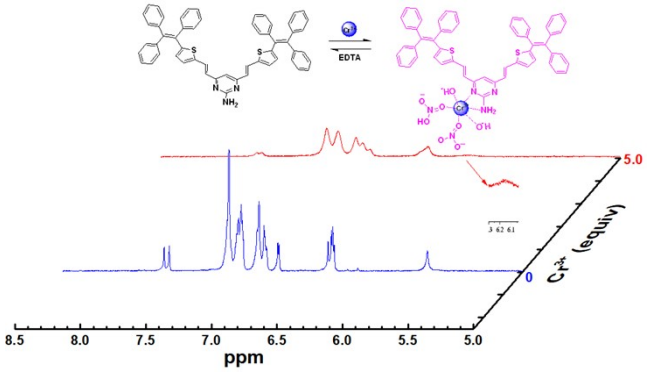

(C)

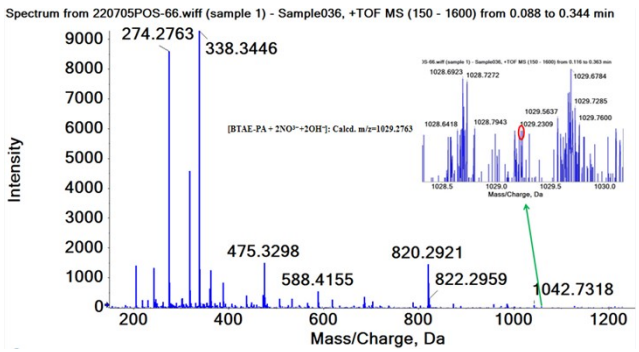

(D)

Figure S11. (A) Hildebrand-Benesi plot based on the 1:1 ratio between **BTAE-PA** and Cr^{3+}, the binding constant for **BTAE-PA** with Cr^{3+} was calculated to be 2.90×10^3 L mol^{-1}; (B) the limit of detection (LOD), LOD is 1.50×10^{-7} mol L^{-1}; (C) Changes in ^1H NMR spectra of **BTAE-PA** stimuli by different Cr^{3+} concentration in THF-d_8, and (D) HRMS-ESI spectra of **BTAE-PA**+Cr^{3+} in acetonitrile.

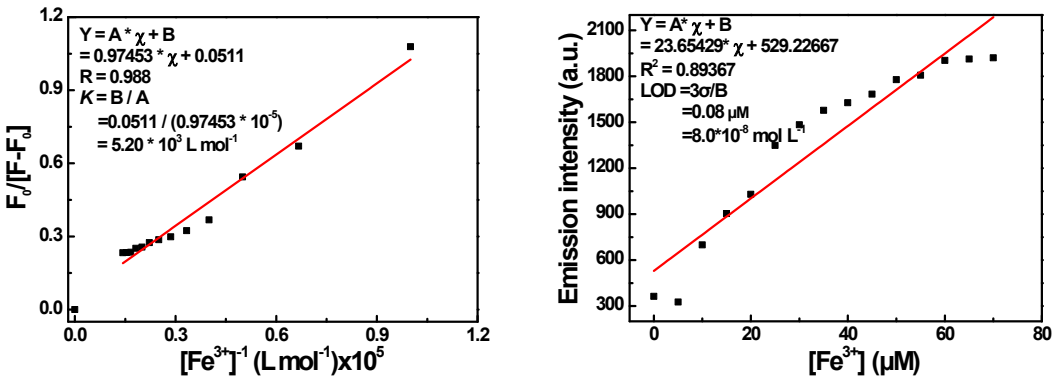

(A) (B)

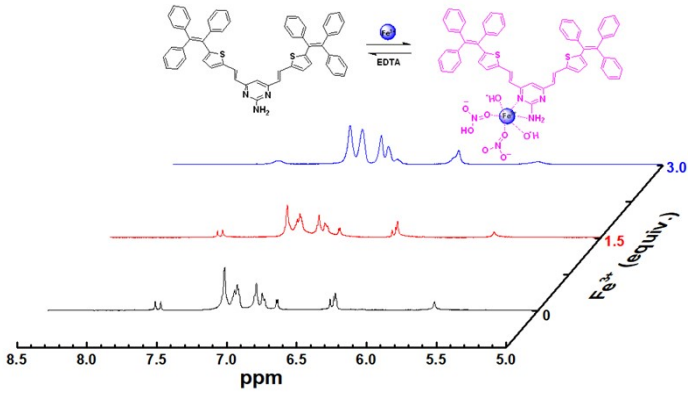

(C)

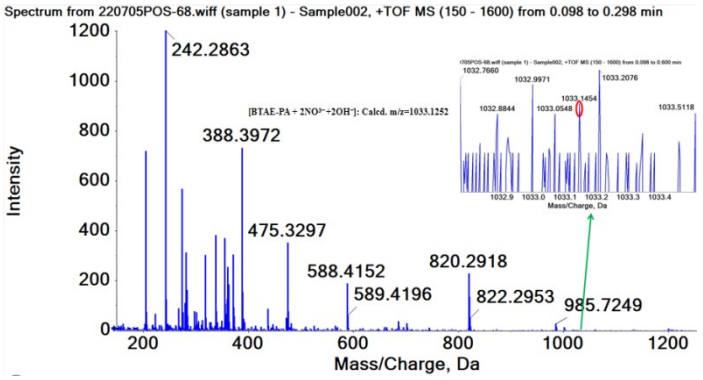

(D)

Figure S12. (A) Hildebrand-Benesi plot based on the 1:1 ratio between **BTAE-PA** and Fe^{3+}, the binding constant for **BTAE-PA** with Fe^{3+} was calculated to be 5.20×10^3 L mol^{-1}; (B) the limit of detection (LOD), LOD is 8.0×10^{-8} mol L^{-1}; (C) Changes in ^1H NMR spectra of **BTAE-PA** stimuli by different Fe^{3+} concentration in THF-d_8, and (D) HRMS-ESI spectra of **BTAE-PA**+Fe^{3+} in acetonitrile.

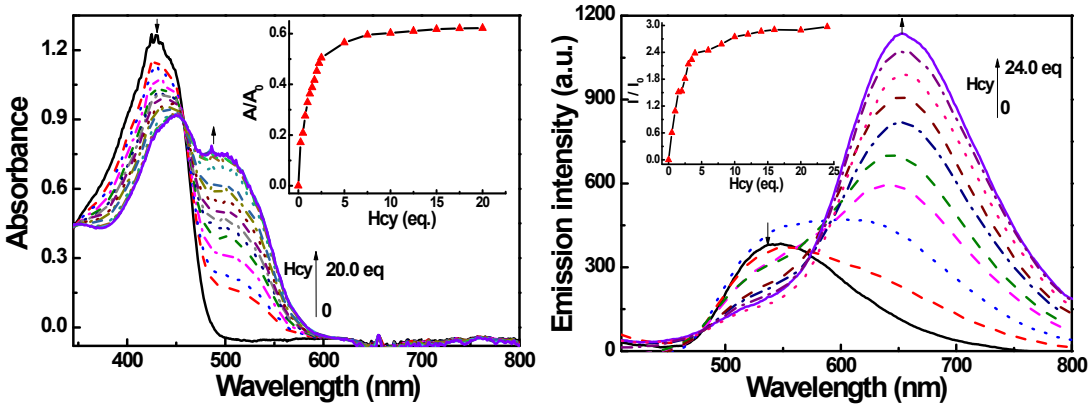

(A) (B)

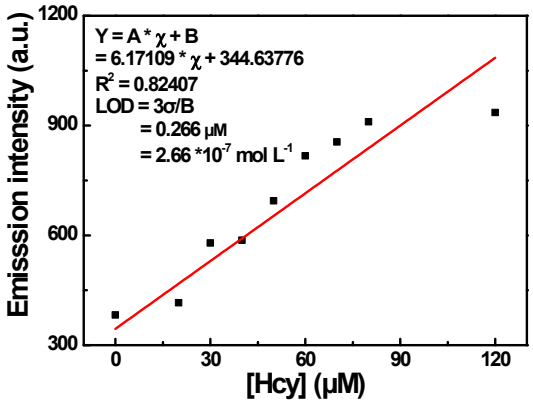

(C)

Figure S13. Absorption and fluorescence spectral changes of **BTAE-PA** by stimulation of Hcy (*C* = 2.0 × 10^{-5} mol L^{-1}): (A) absorption changes (inset: the effect of Hcy concentration on absorption intensity at 486 nm), (B) PL intensity changes (inset: the effect of Hcy concentration on emission intensity at 653 nm, λ_{ex} = 400 nm), and (C) The LOD for Hcy is 2.66 × 10^{-7} mol L^{-1}.

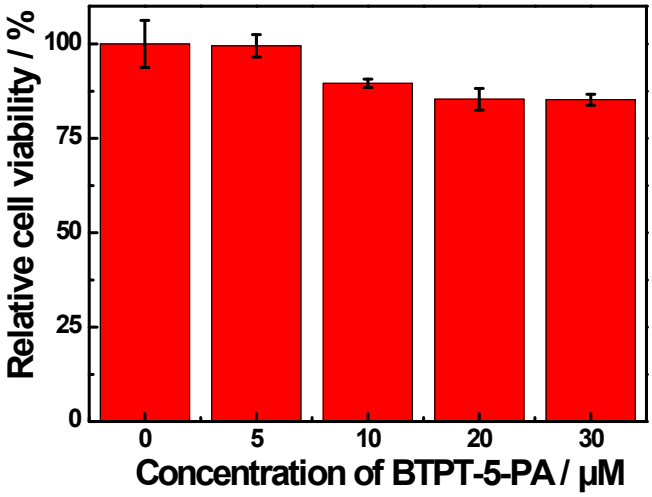

Figure S14. Cytotoxicity of **BTAE-PA** on HeLa cells evaluated by the MTT assay for 24 h.

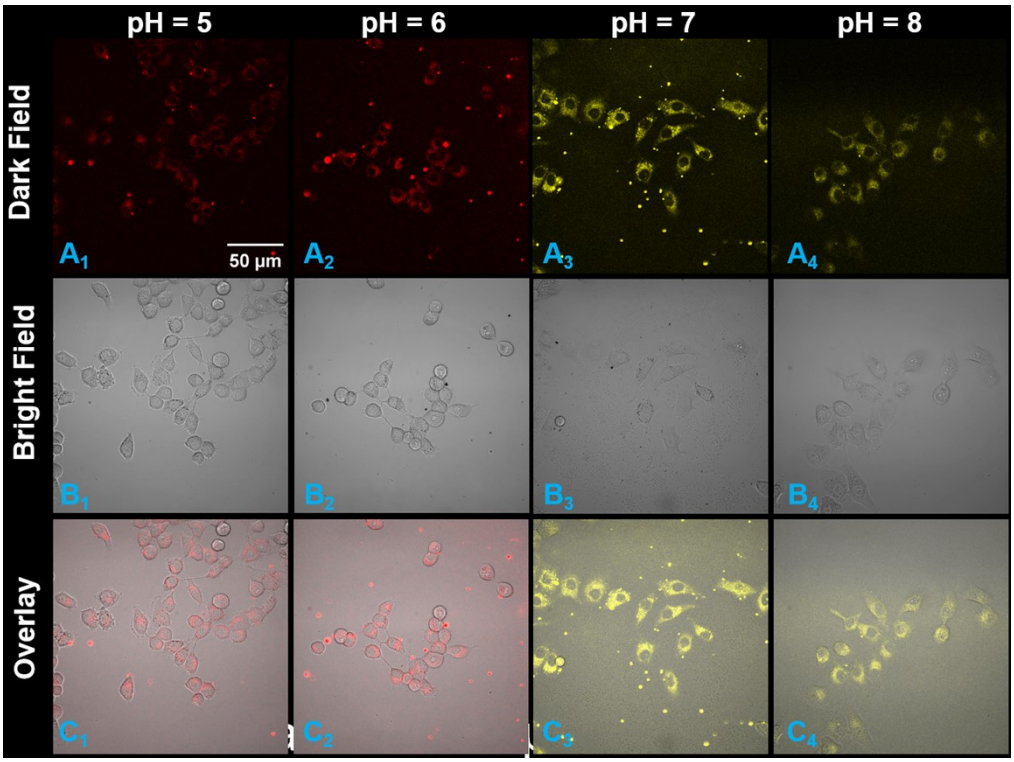

Figure S15. Fluorescent confocal microscopy images of HeLa cells incubated in PBS buffers with various pH (5.0→8.0) and stained with 20 μM of **BTAE-PA**: (A_1–A_4) dark field images, (B_1–B_4) bright field images, (C_1–C_4) overlaid of dark and bright field images, scar bars: 50 μm.

Table S1. The characteristics of **BTAE-PA** in different solvents.

BTAE-PA	*n*-hex	EA	THF	DCM	DMSO	DMF	MeCN	MeOH
Δf^a	0.001	0.201	0.21	0.218	0.263	0.274	0.307	0.309
λ_{abs} (nm)^b	424	426	431	435	435	433	427	435
λ_{em} (nm)^c	538	546	546	566	562	554	568	593
Stokes (nm)^d	114	120	115	131	127	121	141	158
Φ^e	0.017	0.009	0.011	0.008	0.016	0.009	0.007	0.01
ε (mol^{-1} L cm^{-1})^f	6.2×10^4	6.3×10^4	6.1×10^4	6.5×10^4	5.4×10^4	5.6×10^4	6.1×10^4	6.3×10^4

[a] Directed polarizability (Δf); [b] maximum absorption wavelength; [c] maximum emission wavelength; [d] Stokes displacement (nm); [e] fluorescence quantum yield; [f] molar extinction coefficient.

Table S2. Symbolic Z-Matrix of **BTAE-PA**.

C	-10.0816	-6.61102	0.73523
C	-9.76659	-6.27127	-0.58236
C	-8.92488	-5.19214	-0.84494
C	-8.36332	-4.44562	0.20465
C	-8.69904	-4.78981	1.52474
C	-9.54917	-5.86127	1.78714
C	-7.47067	-3.29553	-0.09083
C	-7.92102	-2.4041	-1.19267
C	-6.30922	-3.07688	0.59835
C	-5.69864	-4.11181	1.47975
C	-5.5835	-1.80754	0.50345
C	-5.27443	-3.78605	2.77754
C	-4.69885	-4.75205	3.6011
C	-4.52143	-6.05603	3.13325
C	-4.92214	-6.38632	1.83629
C	-5.50509	-5.42236	1.01682
C	-7.05115	-2.05777	-2.2393
C	-7.48149	-1.23816	-3.27938
C	-8.79059	-0.74835	-3.29247
C	-9.66905	-1.09764	-2.26485
C	-9.24079	-1.92836	-1.22989
C	-6.08246	-0.5211	0.44883
C	-5.08125	0.47051	0.34384
C	-3.79245	-0.03562	0.32277
S	-3.82709	-1.78615	0.44471
C	-2.57977	0.72976	0.23071
C	-2.47179	2.07707	0.18817

C	-1.1967	2.77849	0.09895
N	-1.20024	4.12671	0.08955
C	0.00039	4.72429	0.00284
N	1.2003	4.12561	-0.08586
C	1.19713	2.77742	-0.07457
C	0.00058	2.05449	0.02146
C	2.47145	2.075	-0.16708
N	0.00456	6.0965	0.04945
C	2.57821	0.72748	-0.20565
C	3.7897	-0.03947	-0.29986
C	5.07576	0.46731	-0.38284
C	6.07633	-0.52638	-0.47297
C	5.57984	-1.81479	-0.45418
S	3.82591	-1.79366	-0.34361
C	6.30628	-3.08589	-0.51291
C	7.48854	-3.27085	0.15027
C	5.67276	-4.16109	-1.32739
C	8.37532	-4.43184	-0.11917
C	7.96918	-2.3292	1.19609
C	5.49693	-5.44936	-0.79941
C	4.89273	-6.45078	-1.55617
C	4.45264	-6.18091	-2.85434
C	4.6122	-4.89945	-3.38644
C	5.20916	-3.89582	-2.62548
C	8.96987	-5.12906	0.94604
C	9.8065	-6.21773	0.70774
C	10.08331	-6.61646	-0.60188
C	9.51784	-5.91604	-1.67041

C	8.67276	-4.83507	-1.43169
C	9.28821	-1.85055	1.17184
C	9.74496	-0.9725	2.15423
C	8.89662	-0.57739	3.19051
C	7.58902	-1.06896	3.23918
C	7.13001	-1.93616	2.25125
H	-10.74264	-7.44807	0.94071
H	-10.17915	-6.84547	-1.40714
H	-8.68771	-4.92599	-1.87041
H	-8.2892	-4.20945	2.34435
H	-9.80071	-6.10857	2.81463
H	-5.40994	-2.77153	3.14069
H	-4.38769	-4.48643	4.60738
H	-4.06851	-6.80824	3.77268
H	-4.77646	-7.39526	1.46102
H	-5.81899	-5.67902	0.01028
H	-6.03406	-2.43675	-2.22822
H	-6.79641	-0.9838	-4.08319
H	-9.12511	-0.10642	-4.10232
H	-10.68987	-0.72607	-2.27018
H	-9.92738	-2.2064	-0.43582
H	-7.1441	-0.30985	0.47822
H	-5.28497	1.53495	0.2957
H	-1.66129	0.14785	0.19419
H	-3.36005	2.70442	0.21819
H	0.00058	0.97016	0.02757
H	3.35985	2.70175	-0.20449
H	0.83671	6.54427	-0.3094

H	-0.87025	6.54541	-0.18492
H	1.6593	0.14658	-0.16416
H	5.27766	1.53316	-0.38858
H	7.13597	-0.31493	-0.54368
H	5.84135	-5.65913	0.20801
H	4.76126	-7.44169	-1.13095
H	3.98315	-6.96236	-3.4449
H	4.2705	-4.68073	-4.39411
H	5.33086	-2.89879	-3.03853
H	8.76243	-4.81696	1.96497
H	10.24494	-6.75328	1.54507
H	10.74037	-7.46098	-0.78876
H	9.73955	-6.20935	-2.69266
H	8.2371	-4.29316	-2.2642
H	9.95154	-2.16398	0.37121
H	10.76449	-0.59977	2.11191
H	9.2534	0.10163	3.95958
H	6.92753	-0.77865	4.05052
H	6.11404	-2.31649	2.2881

Table S3. Total energies of **BTAE-PA**.

Zero-point correction	0.809210 (Hartree/Particle)
Thermal correction to Energy	0.860976
Thermal correction to Enthalpy	0.861921
Thermal correction to Gibbs Free Energy	0.711716
Sum of electronic and zero-point Energies	-3118.738773
Sum of electronic and thermal Energies	-3118.687006
Sum of electronic and thermal Enthalpies=	-3118.686062
Sum of electronic and thermal Free Energies=	-3118.836267

Table S4. The photophysical parameters of **BTAE-PA** in different fractions of water (f_w).

f_w	0%	10%	20%	30%	40%	50%	60%	70%	80%	90%
λ_{abs} (nm)[a]	430	433	433	435	433	433	432	466	447	443
λ_{em} (nm)[b]	546	559	561	564	568	573	578	572	586	591
Stokes (nm)[c]	116	126	128	129	135	140	146	106	139	148
Φ[d]	0.011	0.012	0.011	0.015	0.016	0.017	0.016	0.045	0.086	0.144
ε (mol^{-1} L cm^{-1})[e]	6.2×10^4	5.8×10^4	6.3×10^4	6.1×10^4	6.2×10^4	7.0×10^4	6.1×10^4	5.5×10^4	5.3×10^4	4.8×10^4

[a] Maximum absorption wavelength; [b] maximum emission wavelength; [c] Stokes displacement (nm); [d] fluorescence quantum yield; [e] molar extinction coefficient.

Table S5. Photophysical properties of **BTAE-PA** aggregates at different pH.

pH	1	2	3	4	5	6	7	8	9	10	11	12	13
λ_{abs} (nm)[a]	606	448	441	442	439	436	443	442	443	441	443	442	443
λ_{em} (nm)[b]	698	682	659	653	629	612	591	574	571	572	572	573	571
Stokes (nm)[c]	94	234	218	211	190	176	166	132	128	131	129	131	128
Φ[d]	0.058	0.075	0.069	0.089	0.081	0.097	0.144	0.087	0.087	0.086	0.084	0.08	0.076
ε (mol^{-1} L cm^{-1})[e]	2.1×10^4	3.7×10^4	4.3×10^4	4.5×10^4	4.5×10^4	4.4×10^4	4.5×10^4	4.5×10^4	4.5×10^4	4.6×10^4	4.5×10^4	4.4×10^4	4.2×10^4

[a] Maximum absorption wavelength; [b] maximum emission wavelength; [c] Stokes displacement (nm); [d] fluorescence quantum yield; [e] molar extinction coefficient.

Reference

[1] S. Adhikari, S. Ta, A. Ghosh, S. Guria, A. Pal, M. Ahir, et al., A 1,8 naphthalimide anchor rhodamine B based FRET probe for ratiometric detection of Cr^{3+} ion in living cells, *J. Photochem. Photobiol. A: Chem.* 372 (2019) 49-58.